Role of Ethanolamine Utilization and Bacterial Microcompartment Formation in *Listeria monocytogenes* Intracellular Infection

Ayan Chatterjee[a], Karan Gautam Kaval[a]*, and Danielle A. Garsin[a]#

[a]Department of Microbiology and Molecular Genetics, The University of Texas Health Science Center at Houston, Houston, Texas, USA

Running Title: ethanolamine utilization in *L. monocytogenes*

#Address correspondence to Danielle A. Garsin, Danielle.A.Garsin@uth.tmc.edu

*Present address: Department of Molecular Biology, University of Texas Southwestern Medical Center, Dallas, Texas, USA

ABSTRACT

Ethanolamine (EA) affects the colonization and pathogenicity of certain human bacterial pathogens in the gastrointestinal tract. However, EA can also affect the intracellular survival and replication of host-cell invasive bacteria such as *Listeria monocytogenes* (LMO) and *Salmonella enterica* serovar Typhimurium (*S.* Typhimurium). The EA utilization (*eut)* genes can be broadly categorized as regulatory, enzymatic, or structural, and previous work in LMO showed that loss of genes encoding functions for the enzymatic breakdown of EA inhibited LMO intracellular replication. In this work, we sought to further characterize the role of EA utilization during LMO infection of host cells. Unlike what was previously observed for *S.* Typhimurium, in LMO, an EA regulator mutant (*ΔeutV)* was equally deficient in intracellular replication compared to an EA metabolism mutant (*ΔeutB*)*,* and this was consistent across Caco-2, RAW 264.7 and THP-1 cell lines*.* The structural genes encode proteins that self-assemble into bacterial microcompartments (BMCs) that encase the enzymes necessary for EA metabolism. For the first time, native EUT BMCs were fluorescently tagged, and EUT BMC formation was observed in vitro, and in vivo. Interestingly, BMC formation was observed in bacteria infecting Caco-2 cells, but not the macrophage cell lines. Finally, the cellular immune response of Caco-2 cells to infection with *eut* mutants was examined, and it was discovered that *ΔeutB* and *ΔeutV* mutants similarly elevated the expression of inflammatory cytokines. In conclusion, EA sensing and utilization during LMO intracellular infection are important for optimal LMO replication and immune evasion but are not always concomitant with BMC formation.

35 **INTRODUCTION**

36

37 Ethanolamine (EA) is a metabolically useful compound that arises from the membrane lipid
38 phosphatidylethanolamine contained in all bacterial and eukaryotic cells (1, 2). Because of the
39 natural turnover of the epithelium and the cells of the microbiota, the gastrointestinal environment
40 is particularly rich in EA with concentrations as high as 2mM (3, 4). As this compound can serve
41 as a useful source of carbon and/or nitrogen, there is a correlation between bacteria that contain
42 the genes to catabolize this EA and those found in the gut including species of *Enterococcus,*
43 *Escherichia, Clostridium, Salmonella* and *Listeria* (reviewed by (5, 6)). However, expression of
44 the *eut* genes has been documented in other host environments, including the intracellular one,
45 and may be of relevance for *Listeria monocytogenes* (LMO) (7, 8).

46

47 LMO is a facultative, intracellular pathogen, capable of invading, surviving, and multiplying inside
48 various host cell types including cells of the gastrointestinal epithelium and the innate immune
49 cells. Upon attachment, invasion is mediated by engulfment and internalization into a vacuole.
50 Depending on the host cell environment, LMO can disrupt the phagosome, escape into the host
51 cytoplasm, replicate, and spread using actin-based motility (reviewed by (9)). In the host
52 environment of human colon epithelial (Caco-2) cells, a microarray analysis found that the *eut*
53 operon of LMO was upregulated (8). Furthermore, a study of LMO gene expression under several
54 different host conditions, discovered strong upregulation of the *eut* genes in the intestines of
55 infected mice and weaker, but still significant levels of expression in human blood (7).

56

57 The EA utilization genes are usually found together in an operon or locus and encode the
58 necessary regulators, enzymes, and structural proteins (5, 6)). Specifically, *Listeria*
59 *monocytogenes* possesses 17 genes involved in EA metabolism (Fig. 1A) (10). The regulation of

60 the *eut* genes for this bacterium and other Gram-positives such as *Enterococcus* involves an EA-
61 responsive sensor kinase, encoded by *eutW,* a response regulator of the ANTAR family, encoded
62 by *eutV,* and an AdoCbl-dependent riboswitch (10–13). To metabolize EA, an ammonia lyase,
63 composed of two sub-units encoded by *eutBC*, is required for the initial catabolic step that
64 generates acetaldehyde and ammonia. To concentrate these products for the downstream
65 reactions and to prevent interaction of toxic acetaldehyde with the cytoplasm, some, including
66 LMO, also encode for structural proteins that self-assemble into enclosed, proteinaceous
67 structures called bacterial microcompartments (BMCs) (reviewed by (5, 6)).
68
69 In addition to upregulation of the *eut* genes, a contribution of ethanolamine metabolism to LMO
70 intracellular replication in Caco-2 cells was noted; a *eutB* mutant was deficient compared to the
71 parental strain (8). Furthermore, in an intravenous (i.v.) mouse infection model, a *eutB* mutant
72 was deficient in dissemination to the spleen and liver (10). Since EutB is one of the subunits that
73 comprise the ammonia lyase, these data suggest EA catabolism promotes survival in both
74 gastrointestinal epithelial cells and during bloodstream infection (8, 10). Interestingly and in
75 contrast, replication of a *eutB* mutant strain of *Salmonella enterica* serovar Typhimurium was not
76 deficient in host cells. However, replication was diminished for a strain deleted for *eutR*, which
77 encodes the EA-sensing transcriptional regulator (14). This was attributed to the fact that EutR
78 regulates genes associated with pathogenicity in *S.* Typhymurium – the SPI-2 pathogenicity
79 island. Further work by the Kendall group established the importance of the EutH permease for
80 *S.* Typhimurium (15). EutH is required for EA entry under acidic conditions such as those
81 encountered in the phagosome (16). Interestingly, a slight phenotype for a *eutH* mutant in
82 intracellular replication was also shown for LMO, but regulatory or metabolism mutants were not
83 directly compared (15). Whether a LMO *eutV* mutant strain would display a greater deficiency
84 than a *eutB* mutant strain in intracellular replication like *S.* Typhimurium is unknown.

85

86 As mentioned above, EA metabolism is frequently, but not always encased in an organelle-like
87 structure called a bacterial microcompartment (BMC) (reviewed by (6, 17, 18)). Rather than
88 having a selectively permeable membrane, these “organelles” have a selectively permeable
89 protein shell made up of structural components. A feature of the assembly is that some of the
90 enzymatic proteins have “encapsulation peptides” (EPs) that interact with the structural proteins
91 to enable BMC formation. Native EUT BMCs have been visualized in several species of bacteria
92 including LMO by transmission electron microscopy (TEM) (19). However, fluorescent-tagging of
93 EUT BMCs to our knowledge was only done in a heterologous system in which *eut* genes
94 encoding the structural proteins of *S.* Typhimurium were over-expressed in *E. coli* using a
95 constitutively active promoter, and BMCs were visualized by tagging an encapsulation peptide
96 with GFP (20–22). Here we report the fluorescent tagging of native EUT proteins under the control
97 of *eut* promoters to permit the visualization of endogenous BMC formation in vitro and in host
98 cells.

99

100 In this work, we sought to further characterize the role of EA utilization during LMO infection of
101 host cells. Unlike what was previously observed with *S.* Typhimurium (14), an EA metabolism
102 mutant (*ΔeutB*) was equally deficient in intracellular replication compared to an EA regulator
103 mutant (*ΔeutV),* and this was consistent across a number of cell types. To visualize EUT BMC
104 formation, native structural proteins were fluorescently tagged and expressed under *eut*
105 promoters. EUT BMC formation was observed in vitro, and for the first time, in vivo, in some, but
106 not all host cells tested. Finally, it was found that LMO *ΔeutB* and *ΔeutV* mutants similarly affected
107 the cellular immune response; comparable increases in several inflammatory cytokines were
108 observed.

RESULTS

Establishment of conditions in which LMO can utilize ethanolamine (EA) as a nitrogen source dependent on the *eut* genes:

Previous work demonstrated that LMO can utilize EA as a source of carbon and/or nitrogen dependending on the media conditions (19, 23). We optimized a similar chemically defined medium that we named MMWB (Modified MWB) (Table S1) (24–27). MMWB contained 4.1mM glutamine (Gln) as the nitrogen source allowing for robust growth of LMO (Fig. 1B). EA could be substituted for Gln, which requires the bacteria to utilize EA as a nitrogen source. As expected, no growth was observed in the absence of Gln, underscoring the necessity of a nitrogen source (Fig. 1B). To testif EA could substitute as a nitrogen source in the medium, we replaced Gln with 16mM EA. However, no growth was observed until we additionally supplemented the medium with 200μM of AdoCbl (Fig. 1B). The data aligns with previous research demonstrating a requirement for AdoCbl as a co-factor in the metabolism of EA and in the induction of the *eut* genes (reviewed by (6)). In conclusion, we show that LMO can grow in MMWB utilizing EA as a nitrogen source.

As described in the introduction and illustrated in Fig. 1A, the *eut* locus of LMO contains 17 genes that encode the regulators, enzymes and structural shell proteins necessary for EA metabolism. To verify induction of these genes in MMWB + EA, expression of a subset was measured by qRT-PCR. As expected, all genes measured, *eutV, A, B, K,* and *M,* displayed increased expression following 4 hours of growth in MMWB + EA relative to MMWB + Gln. Of note, the expression was specific for *eut* genes associated with EA metabolism; genes associated with propanediol (PDU) metabolism, *pduA* and *pduQ,* were not induced (Fig 1C).

134 To further verify the role of the *eut* genes in LMO's use of EA as a nitrogen source in MMWB, we
135 generated strains containing *ΔeutV* (LMAC030) and *ΔeutB* (LMAC031) non-polar, in-frame,
136 deletion mutations in the parental background (Fig 1D and 1E). When grown in the presence of
137 Gln as the nitrogen source, these mutant strains exhibited growth comparable to the parental
138 strain. However, they did not grow when EA was provided as a nitrogen source, indicating that
139 the response regulator, EutV, and the ammonia lyase subunit, EutB, were indispensable for
140 growth in the presence of EA in vitro, as expected. To ensure that the defects in growth were due
141 to the introduced mutations, we complemented these strains. In order to retain EA-inducibility, the
142 complementation constructs included the regulatory sequences upstream of *eutV* or *eutG.* Both
143 these regions contain predicted promoters followed by ANTAR binding sites that are the hallmarks
144 of antitermination regulation by EutV (Fig 1A) (10). Growth in EA was partially restored for the
145 *ΔeutV* strain when *eutV,* under the control of the *eutV* promoter, was introduced as a transgene
146 into a chromosomal site outside of the EA locus (see Materials and Methods for details), (Fig 1D
147 and S1A). Note that successful complementation of *ΔeutV* required using the combined *eutVW*
148 sequence; attempts to complement with the *eutV* sequence alone were unsuccessful. As the *eutV*
149 and *eutW* genes overlap and appear to be co-transcribed, it is possible that a *eutV* transcript
150 alone is unstable. Growth in EA was also restored in the *ΔeutV* background, but to a lesser
151 degree, when the *eutG* promoter was utilized (Fig S1A). In contrast, successful complementation
152 was only achieved in the *ΔeutB* strain with the *eutG* promoter driving the expression of *eutB*; use
153 of the *eutV* promoter did not enable growth in EA (Fig 1E and S1B). We speculate that these
154 differences in the promoters' abilities to restore growth in EA is due to differences in the levels of
155 EutV and EutB that are required for EA metabolism and achieved by the promoters. Overall, these
156 results establish conditions in which LMO can utilize EA as a source of nitrogen dependent on
157 the positive regulation of the *eut* genes (EutV) and the ability to metabolize EA (EutB).
158

159 **LMO EUT BMC formation is dependent on EA, EutV, and EutB:**

160 EA utilization of has been associated with BMC formation for many EA-utilizing bacteria including
161 *L. monocytogenes* (6, 19). Specifically, LMO EUT BMCs were previously visualized under
162 anaerobic conditions (19). To test for BMC formation in aerobic MMWB + EA conditions,
163 transmission electron microscopy (TEM) was utilized. Structures resembling BMCs were readily
164 visible in the parental LMO background following 6 hours growth in medium containing EA but not
165 Gln (Fig. 2A). As dependence of the formation of these structures on EutV and EutB had not
166 been previously reported in LMO, we also examined *ΔeutV* and *ΔeutB* deletion mutant strains
167 grown in EA; both strains failed to form BMCs (Fig. 2B and 2C). The complemented strains both
168 restored BMC formation, as predicted, indicating that the deletions did not have polar effects on
169 the expression of the downstream structural genes (Fig. 2B, 2C and 1A).

170

171 In order to visualize EUT BMC formation in live cells, we introduced a *eutK::mCherry* translational
172 fusion under the control of the EA inducible *eutG* promoter into an ectopic, chromosomal site in
173 wild-type, *ΔeutV* and *ΔeutB* backgrounds (see Materials and Methods). To ensure that
174 introduction of the protein fusion did not disrupt the ability of the strain to utilize EA, growth curves
175 were performed, and the strain was found to grow in EA with kinetics similar to the parental strain
176 (Fig. S1C). Following six hours of incubation in medium containing EA, distinct red punctate
177 structures were observed corresponding to BMC-like formations (Fig. 3A). Notably, when bacterial
178 cells were cultivated in a medium containing Gln, these BMC-like structures were not evident
179 under confocal microscopy. (Fig. 3B). By performing live cell imaging of this strain, the dynamics
180 of these structures forming and dissipating was revealed (Mov. S1). Consistent with the TEM
181 observations, BMCs were rarely visible in the *ΔeutV* and *ΔeutB* strain backgrounds (Fig. 3C and
182 3D). In addition to the *eutK::mCherry* translational fusion, *eutM::mCherry* and a
183 *eutK::mNeonGreen* fusions were additionally generated. They presented with a similar punctate

184 fluorescent pattern when grown in EA, indicating that the observed localization was unlikely to be
185 artifactual due to a specific fusion or tag (S2A and S2B). In conclusion, these experiments
186 demonstrate that EUT BMC formation is dependent on EA, EutV, and EutB and can be visualized
187 with fluorescent tags in *L. monocytogenes*.
188
189 **Loss of EA utilization impairs intracellular replication of LMO:**
190 As LMO invades the cells of the gastrointestinal epithelium in humans, the Caco-2 human
191 colorectal adenocarcinoma cell line is frequently used to model LMO intracellular infections (28,
192 29). Previous work on strain LMO EGDe documented that a strain with an insertion mutant in *eutB*
193 was deficient in Caco-2 intracellular replication (8). To verify the phenotype with LMO 10403S,
194 we infected Caco-2 cells with the parental strain and the *ΔeutV* and *ΔeutB* strains. Following a
195 one-hour infection at an MOI of 5, the cells were washed, and medium containing gentamycin
196 was added for one hour to kill extracellular bacteria. At the zero-time point, defined as when the
197 extracellular bacteria were removed and the cells washed, the number of intracellular bacteria
198 between the strains was not significantly different, indicating no defect in bacterial invasion (Fig.
199 4A). However, at three hours post-infection, there was approximately half-a-log less CFU of the
200 *ΔeutV* and *ΔeutB* strains compared to wild type, demonstrating a defect in intracellular replication.
201 We additionally observed that there was no significant difference in the level of attenuation
202 between the two mutant strains.
203
204 Following enterocyte invasion, *L. monocytogenes* can infect recruited immune cells such as
205 macrophages, which can lead to systemic infections (9). A LMO mutant in *eutH,* which encodes
206 for an EA transporter thought to be necessary for EA utilization in acidic environments, was
207 previously shown to have a slight defect in intracellular replication in bone marrow-derived
208 macrophages (BMDMs), suggesting that EA utilization might play a role in this process (15). To

209 further test the efficiency of intracellular replication of the *eut* mutant strains in immune cells, we
210 infected RAW 264.7 and differentiated THP-1 cells, mouse and human derived macrophages
211 respectively (Fig. 4B and 4C). Replication of the *ΔeutV* and *ΔeutB* strains was attenuated by
212 about 0.5 logs in these cells. Again, there was no significant difference in the degree of deficiency
213 between the two strains. In conclusion, the *ΔeutV* and *ΔeutB* strains are deficient in intracellular
214 replication to an equal degree in a range of cell types suggesting that EA utilization positively
215 contributes to LMO infection efficiency.
216
217 **LMO forms EUT BMCs during intracellular infection of Caco-2 cells:**
218 To test for BMC formation in the intracellular environment, Caco-2 cells were infected with the
219 strains expressing the *eutK::mCherry* fusion. Strains containing the *eutK::mCherry* translational
220 fusion were utilized for the in vivo experiments because they were brighter compared to the
221 *eutM::mCherry* strains (Fig. S2A) and were less prone than mNeonGreen to interference from
222 background autofluorescence (Fig. S2B). The samples were fixed at 2-, 4-, 6- and 8-hours post-
223 infection, and bacterial cells were visualized using an antibody specific to *L. monocytogenes.* Host
224 cell actin was visualized by staining with phalloidin. At 4, 6, and 8 hours, punctate, red
225 fluorescence inside some of the bacterial cells from the parental strain was visible, indicative of
226 BMC formation (Fig. 5A and Fig. S3). As expected, little to no signal was observed in samples
227 from the *ΔeutV* and *ΔeutB* strains containing the *eutK::mCherry* fusion (Fig. 5B-C and Fig S3).
228 The number and the intensity of the punctate, red fluorescence in the parental strain cells
229 increased over time, peaking at 8 hours (Fig. 5A). Time points later than 8 hours were not captured
230 due to host cell lysis. However, as shown by imaging the larger fields (Fig. S3), not all bacteria
231 within the host cells presented with visible BMCs, and while the host cells were stained with actin,
232 we did not observe actin clouds or tails around the bacterial cells, hallmarks of *L. monocytogenes*
233 escape into the host cell cytoplasm (9). Our Caco-2 cells were not highly passaged, and our

234 observations align with the published literature asserting that only highly passaged strains of
235 Caco-2 cells are conducive to *L. monocytogenes* phagosomal escape (29, 30). From these data
236 we conclude that the *eut* genes are expressed and EUT BMCs form in *L. monocytogenes* inside
237 Caco-2 cells.
238
239 Confocal imaging was also performed on RAW 264.7 cells infected with the *eutK*-mCherry strain.
240 Time points were taken at 4, and 6 hours; later time points were not possible due to cell lysis.
241 Unlike Caco-2 cells, phagosomal escape was evident by the formation of actin clouds and tails
242 visualized by staining with phalloidin (Fig. S4A). However, despite the *eut* genes contributing to
243 higher intracellular replication in these cells (Figure 3B), we were unable to detect any mCherry
244 signal. To test if the lack of visible staining was due to an absence of BMC formation as a result
245 phagosomal escape, we differentiated THP-1 monocytes into the M1 phenotype, previously
246 shown to prevent phagosomal escape of LMO (31). When infected with LMO, there was no
247 evidence of cytoplasmic LMO as indicated by actin cloud or tail formation. However, no mCherry
248 expression indicative of BMC formation was visible (Fig. S4B). These results suggest that the
249 presence or absence of visible BMCs is unrelated to phagosomal escape.
250
251 **Loss of EA utilization increases host cell inflammatory responses:**
252 To further investigate the role of EA utilization in LMO's interaction with host cells, we examined
253 the inflammatory response of Caco-2 cells following infection. Specifically, the expression of
254 genes encoding for inflammatory cytokines, vital signaling mediators that orchestrate and amplify
255 the immune response by recruiting immune cells and enhancing antimicrobial capabilities, were
256 measured (32, 33). Caco-2 cell cultures were subjected to infection with the LMO parental or the
257 *ΔeutV* and *ΔeutB* mutants as before, and host cell RNA was extracted at four hours post-infection.
258 The expression levels of specific inflammatory cytokines, interleukin-1 beta (IL-1β), tumor

259 necrosis factor-alpha (TNF-α), interleukin-6 (IL-6), interleukin-8 (IL-8), and chemokines CXCL2
260 and MCP-1 were examined by qRT-PCR as described previously for Caco-2 cells (34). A 2-4-fold
261 increase in the expression of these factors by Caco-2 cells infected with the *ΔeutV* and *ΔeutB*
262 mutant strains was observed in comparison to those infected with the parental strain (Figure 6).
263 There were no significant differences in the expression levels of these cytokines between the
264 *ΔeutV* and *ΔeutB* mutant strains, suggesting that the observed differences are solely due to the
265 loss of ethanolamine utilization. The stronger inflammatory response coupled with the reduced
266 intracellular replication observed during infection with the mutant strains (Figure 3A) suggests that
267 loss of ethanolamine utilization reduces LMO's ability to evade the host immune response.

268 **DISCUSSION**

269

270 In this study, we demonstrated that the catabolism of EA contributes to the efficacy of intracellular
271 replication of LMO in a variety of host cells. In *S.* Typhimurium, by contrast, the ability to sense,
272 but not catabolize EA, was shown to enhance intracellular survival in macrophages; a *eutR*
273 regulatory mutant was deficient in intracellular survival, but a *eutB* metabolic mutant was *not.* (14).
274 Here, a direct comparison between LMO *eutV* regulatory and *eutB* metabolic mutants revealed
275 indistinguishable phenotypes, both exhibited the same level of depressed intracellular replication
276 and caused similar changes to the host cell immune response (Fig. 3 and 6). The difference could
277 be related to the scope of the genes regulated by EutR and EutV. EutR is a DNA binding
278 transcriptional regulator. In addition to binding its promoter in the *eut* locus, EutR directly binds
279 the promoter of the *ssrB* gene in *S.* Typhimurium encoding a transcriptional regulator. SsrB
280 activates the expression of the Salmonella pathogenicity island 2 (SPI-2) genes that are required
281 for *S*. Typhimurium intracellular replication and survival (14). EutR in EHEC also regulates
282 virulence related genes outside of the *eut* locus (35, 36). In contrast, EutV is an ANTAR (AmiR
283 and NasR transcriptional antiterminator regulators) response regulator that binds specific
284 sequences in mRNA leaders that overlap terminators, preventing their formation (37, 38) In LMO,
285 there is no evidence that EutV directly regulates genes other than those related to EA utilization
286 (10, 37). The observation that strains containing *eutV* and *eutB* deletions cause identical effects
287 on LMO intracellular replication as well as on host cell immune responses is consistent with the
288 phenotypes being caused by the loss of the ability to catabolize EA in this bacterium, unlike in *S.*
289 Typhimurium. How exactly the loss of EA metabolism causes these changes in LMO's
290 interactions with host cells is of future interest.

291

292 By fluorescently tagging BMC structural proteins, we were able to visualize BMC formation in vitro
293 and in vivo. The goal was to observe the formation of BMCs as a marker for when and where EA
294 metabolism occurs during LMO interaction with host cells. However, we observed BMCs forming
295 in only a subset of the bacteria inside Caco-2 cells, and we did not observe any forming in the
296 RAW 264.7 and THP-1 cell lines. Based on the data, we postulate two possible explanations for
297 the lack of visible BMC formation in these monocyte/macrophage cell lines. One is that, that BMCs
298 were generated, but were unable to be visualized due to low expression of the *eutK::mCherry*
299 transgene. Another is that the metabolism of ethanolamine is occurring at a lower level in these
300 cells that does not require BMC formation. Recall that some bacterial species, like *Pseudomonas*
301 *aeruginosa* and *Acinetobacter baumannii* encode for the core EA metabolic enzymes, but lack
302 the structural proteins (38, 39). Even in bacteria such as *S. typhimurium* that contain the full
303 complement of structural proteins, it has been shown that they are still able to metabolize EA,
304 albeit with less efficiency, when they are deleted for the microcompartment-encoding genes (40,
305 41). Perhaps there are differences in the amount of free EA available in these different host cells
306 that determine whether BMC formation is necessary for EA utilization or not. Future work using
307 transcriptomics and metabolomics to further understand the host cell environments and the
308 bacterial response may provide more insight into these observations.
309
310 Another surprising finding in this study was the lack of BMC formation in the *ΔeutB* mutant. We
311 expected that no structures would form in the *ΔeutV* mutant that lacks the regulator necessary for
312 expression of all the *eut* genes but were surprised that a strain missing a single catalytic enzyme
313 failed to form BMCs. However, it has been reported that the shell proteins of the carbon-fixing β-
314 carboxysomes condense around key catalytic enzymes necessary for nucleation of the BMC
315 structure (18, 42). In contrast, the α-carboxysomes can assemble either shell-first or undergo
316 concomitant shell–core assembly, and the propanediol (PDU) metabolizing BMCs form

317 independent cargo and shell aggregates (43–45). While there have been studies in heterologous
318 systems to examine the requirements for EUT BMC assembly (20–22), the dynamics have not
319 been determined in a natural system. Therefore, it is possible that core assembly requiring EutB
320 is necessary for shell protein condensation. However, our previous work in *E. faecalis*
321 documented normal BMC formation by TEM in strains with *eutB* mutations (46), raising the
322 possibility of species-specific differences. Undoubtedly, it will be of interest to further study EUT
323 BMC formation and elucidate the assembly pathway(s). More broadly, the field should investigate
324 if the assembly of BMCs varies in a manner dependent on species and environmental context,
325 including host environments. In conclusion, EA utilization contributes importantly to LMO
326 intracellular replication, but may not always require EUT BMC assembly.

327 **MATERIALS AND METHODS**

328

329 **Bacterial strains and media**

330 *Listeria monocytogenes* 10403s (LMO) strain (source: Bei resources) was used in this study and
331 all mutations and recombinants were constructed in this background. All LMO strains were grown
332 in brain heart infusion (BHI) broth or on BHI agar (1.5% agar) plates supplemented with
333 streptomycin (50 µg /ml) in 37 °C. The chemically defined medium MMWB (Table S1) was
334 prepared by modifying the original recipe reported by Welshimer (24). Medium was always
335 prepared fresh, and filter sterilized with a 0.22micron filter. MMWB medium was supplemented
336 with either glutamine (Gln: 4.1mM) or ethanolamine (EA: 16mM) and VitB12 (200µM) as needed.
337 Cloning was done in either *E. coli* Top10 or DH5α. All *E. coli* strains were grown in Luria-Bertani
338 (LB) broth and were supplemented with antibiotics [Ampicillin (100 µg /ml) or Kanamycin (50
339 µg/ml)] wherever required. For recombinant LMO strains, appropriate antibiotics [Kanamycin (50
340 µg/ml) and streptomycin (50 µg/ml)] were used.

341

342 Generation of recombinant, *ΔeutV*, *ΔeutB* and the various complemented strains in LMO
343 All primers used in this study were purchased from Sigma-Aldrich and are listed in Table S2. PCR
344 reactions were performed using Platinum™ SuperFi II DNA Polymerase (ThermoFisher Scientific:
345 12361010) according to the manufacturer's protocol. Restriction free cloning was conducted using
346 NEBuilder® HiFi DNA Assembly (NEB: E2621L). Isolation of plasmids and purification of PCR
347 products were conducted by using commercially available kits from either Qiagen or Macherey-
348 Nagel. Sequencing was conducted at Genewiz, and the results visualized and verified using
349 SnapGene (version 5.2.5.1). For creating the *ΔeutV* (LMAC030) and *ΔeutB* (LMAC031), the
350 respective upstream and downstream regions were cloned into pMAD and electroporated into
351 LMO as reporter earlier (47). Electrocompetent cells of LMO were prepared as described (48).

352 The complemented strains *ΔeutV::eutV* (LMAC037) *and ΔeutB::eutB* (LMAC034) were created
353 by cloning the respective gene along with promoter region of either *eutV* or *eutG* in pIMK plasmid
354 followed by electroporation. For creating the recombinant strain expressing mCherry tagged to
355 EutK (LMAC038), the *eutK* coding sequence was driven by the *eutG* promoter and fused to the
356 mCherry coding sequence. It was then cloned into the pIMK plasmid to create the construct
357 AC038 followed by electroporation as described by Monk *et al*, 2008. Similarly, AC038 was
358 electroporated into LMAC030 (*ΔeutV*) and LMAC031 (*ΔeutB*) to generate strains LMAC040
359 (*eutK::mCherry*; *ΔeutV*) and LMAC043 (*eutK::mCherry*; *ΔeutB*), respectively.
360
361 **Growth curves**
362 LMO and the mutants were grown overnight in 10 ml of BHI broth at 37°C with aeration. Bacterial
363 cells were harvested and washed thrice with PBS followed by a wash with MMWB medium devoid
364 of glutamine or EA. Cultures were then seeded on a 48 well plate from Falcon® (Corning)
365 containing the desired medium with a starting OD_{600} of 0.05. Plates were sealed with Breathe-
366 Easy® sealing membranes (Diversified Biotech) and the growth curve was monitored on a
367 Cytation™ 5 plate reader system (BioTek Instruments Inc) for 72 hours, with OD readings taken
368 every hour.
369
370 **Transmission Electron Microscopy**
371 Bacterial strains were grown in BHI broth to midlog phase at 37°C with aeration. Bacterial cells
372 were then harvested, washed, and processed as mentioned above. The strains were
373 resuspended in MMWB medium containing either Gln (4.1mM) or EA (16mM) and Vit B12
374 (200μM) as needed. Cells were then harvested, fixed, processed and sliced (12). Imaging was
375 conducted in JEOL 1400 TEM system, equipped with the Gatan 2k x 2k CCD camera, and
376 accompanying software.

377

378 **Cell culture and infection**

379 All the cell lines were purchased from Sigma. The murine macrophage RAW264.7 cell line and
380 Human colon adenocarcinoma Caco-2 cell line was cultured in DMEM (Gibco: 11995065)
381 supplemented with 10% fetal bovine serum (FBS) (Gibco: 10082147) at 37°C in a humidified
382 atmosphere at 5% CO_2. For culturing the Caco-2 cell line, DMEM medium was additionally
383 supplemented with non-essential amino acids (NEAA) (Gibco-11140050). The human monocytic
384 leukemia THP-1 cell line was thawed and cultured in RPMI media supplemented with 20% FBS
385 and 2-mercaptoethanol (Gibco: 21985023) to a final concentration of 0.05 mM at 37°C in a
386 humidified atmosphere at 5% CO_2. Once the culture was established, the FBS concentration was
387 reduced to 10% for further subculturing. PMA was used at a final concentration of 1000ng/ml for
388 48 hours to differentiate the THP-1 cells. This was followed by incubating the differentiated THP-
389 1 cell in PMA free media for 24hr. Polarization of the differentiated THP-1 macrophages to M1
390 phenotype was done by adding 10ng/ml LPS and 50ng/ml IFN-γ (31). For RAW264.7 and THP-1
391 macrophage intracellular survival assay, 5 x 10^5 cells were seeded into 12 well plates the day
392 before the experiment. For Caco-2 cells, 5 x 10^5 cells were seeded into 12 well plates and allowed
393 to grow for two weeks until tight junctions were formed (49). LMO strains were grown overnight in
394 BHI broth at 37°C. The next day the overnight cultures were inoculated into fresh BHI to a starting
395 OD_{600} of 0.05 and grown for 2 h at 37°C till an OD_{600} of ~0.2. Cell lines were infected with a MOI
396 of 5. The infection was conducted for 1 hour. The wells were then washed with Dulbecco's
397 phosphate-buffered saline (PBS) (prewarmed at 37°C), and extracellular bacteria were killed by
398 incubating with DMEM containing 40 µg/ml gentamicin for 1 hour. Medium was changed after 1
399 hour and intracellular bacteria was harvested by lysing the host cells with 1 ml of ice-cold PBS
400 containing 0.1% Triton X-100. Several serial dilutions were plated on BHI agar plates and kept at

401 37°C for the bacterial colonies to appear. Colonies were counted manually as well as using the
402 software openCFU (version 3.9.0) (Geissmann, 2013).
403
404 **cDNA preparation and qRT PCR**
405 All RNA extraction was carried out using NucleoSpin RNA Plus kit (Macherey Nagel) according
406 to manufacturer's protocol. cDNA was synthesized from RNA using the RevertAid reverse
407 transcriptase for first strand cDNA synthesis (ThermoFisher Scientific: K1622). qRT-PCR was
408 performed using SYBR green based iTaq Universal SYBR Green Supermix (Biorad: 1725121),
409 using appropriate primers (Table S2) on a Biorad C1000 thermocycle equipped with CFX96
410 Optical Reaction Module. The relative expression of various genes was normalized to that of the
411 endogenous reference 16S rRNA gene and the fold change in expression was calculated using
412 the comparative Ct method. For host qRT-PCR, the normalization was done using ACTH as
413 endogenous reference. p-values were calculated using the Two-way ANOVA with Bonferroni's
414 multiple comparison test.
415
416 **Confocal microscopy**
417 To visualize the expression of EutK-mCherry, the recombinant LMO strains LMAC038
418 (*eutK::mCherry)*, LMAC040 ((*eutK::mCherry*; *ΔeutV*) and LMAC043 (*eutK::mCherry; ΔeutB*),
419 were initially grown overnight in BHI broth at 37°C. Bacterial cells were then washed with sterile
420 PBS and reconstituted in MMWB medium containing either Gln (4.1mM) or EA (16mM) and VitB12
421 (200μM) as needed and incubated at 37°C on a shaker (180 rpm). Cells were harvested by
422 centrifugation (5000x g) at desired timepoints and were fixed with 4% paraformaldehyde for 10
423 minutes at 25°C. Cells were then washed thrice with PBS and smear dried on a Poly-L-lysine
424 coated slide (Electron Microscopy Science: 63410), mounted with Prolong Diamond Antifade
425 Mountant (Invitrogen: P36965), covered with #1.5H glass cover slips (Electron Microscopy

426 Sciences), and imaged using the Olympus FLUOVIEW FV3000 confocal microscope equipped
427 with the Fluoview FV315-SW software. Images were acquired in Z-stacks using a step size of
428 0.20 µm, which were then processed using the Olympus cellSens Dimension software.
429
430 Caco-2, RAW264.7 and THP-1 cells were thawed and seeded as mentioned earlier on 6 well
431 plates containing #1.5H glass cover slips (Electron Microscopy Sciences). Cells were grown and
432 maintained as described above. The infection was conducted for 1 hour at an MOI of 5, followed
433 by gentamycin treatment as described above. After infection, the cells were fixed with 4%
434 paraformaldehyde for 10 minutes at 25°C followed by permeabilization with 0.01% Triton X-100
435 in PBS for 10 minutes at 25°C. The cells were then treated with 5% BSA in PBS for 90 minutes
436 at 25°C followed by treatment with anti-Listeria antibody (Abcam: ab35132) at 4°C overnight. The
437 next day, cells were then washed with PBS and treated with Alexa488 conjugated secondary
438 antibody (Invitrogen: A27034) for 90 minutes at 25°C. Cells were then washed and stained for
439 actin using Alexa Fluor plus 405 Phalloidin (Invitrogen: A30104) for 20 minutes at 25°C. Finally,
440 cells were again washed with PBS, mounted, and imaged as described above.
441
442 **Statistical Analysis**
443 Statistical Analyses were done using GraphPad Prism, v9.5.1. P values were calculated using
444 two-way ANOVA with Bonferroni's multiple comparison test.
445
446 **Data Availability**
447 No large datasets were generated that required deposition into public repositories. All data is in
448 the manuscript with the source data underlying the Figures is in Table S3.
449
450 **ACKNOWLEDGEMENTS**

We thank S. Kolodziej and P. Navarro for sectioning samples for TEM. We also thank Dr. Chenggang Wu and Ms. Mara Blaise Willis for help with strain design and troubleshooting. Finally, we thank the following members of the LMO community for strains, protocols and advice: D. Portnoy, J.D. Sauer, S. Halbedel and M. O'Riordan. This work was supported by the National Institute of Allergy and Infectious Diseases of the National Institutes of Health under award number R21AI167124 to DAG. The content is solely the responsibility of the authors and does not necessarily represent the official views of the National Institutes of Health. Author contributions: A.C., K.K., and D.A.G. designed research; A.C and K.K performed experiments; A.C and D.A.G analyzed data and wrote the paper.

461 **BIBLIOGRAPHY**

462

463 1. Randle CL, Albro PW, Dittmer JC. 1969. The phosphoglyceride composition of Gram-
464 negative bacteria and the changes in composition during growth. Biochim Biophys Acta
465 187:214–220.

466 2. White DA. 1973. Phospholipid composition of mammalian tissues, p. 441–482. *In* Ansell,
467 GB, Hawthorne, JN, Dawson, RMC (eds.), Form and function of phospholipids. Elsevier
468 Publishing Company, New York.

469 3. Bertin Y, Girardeau JP, Chaucheyras-Durand F, Lyan B, Pujos-Guillot E, Harel J, Martin
470 C. 2011. Enterohaemorrhagic Escherichia coli gains a competitive advantage by using
471 ethanolamine as a nitrogen source in the bovine intestinal content. Environ
472 Microbiol2010/09/21. 13:365–377.

473 4. Thiennimitr P, Winter SE, Winter MG, Xavier MN, Tolstikov V, Huseby DL, Sterzenbach T,
474 Tsolis RM, Roth JR, Baumler AJ. 2011. Intestinal inflammation allows Salmonella to use
475 ethanolamine to compete with the microbiota. Proc Natl Acad Sci U S A2011/10/05.
476 108:17480–17485.

477 5. Garsin DA. 2010. Ethanolamine utilization in bacterial pathogens: roles and regulation. Nat
478 Rev Microbiol 8:290–295.

479 6. Kaval KG, Garsin DA. 2018. Ethanolamine Utilization in Bacteria. mBio 9.

480 7. Toledo-Arana A, Dussurget O, Nikitas G, Sesto N, Guet-Revillet H, Balestrino D, Loh E,
481 Gripenland J, Tiensuu T, Vaitkevicius K, Barthelemy M, Vergassola M, Nahori MA,
482 Soubigou G, Regnault B, Coppee JY, Lecuit M, Johansson J, Cossart P. 2009. The Listeria
483 transcriptional landscape from saprophytism to virulence. Nature.

484 8. Joseph B, Przybilla K, Stuhler C, Schauer K, Slaghuis J, Fuchs TM, Goebel W. 2006.
485 Identification of Listeria monocytogenes genes contributing to intracellular replication by
486 expression profiling and mutant screening. J Bacteriol 188:556–568.
487 9. Pizarro-Cerda J, Cossart P. 2018. Listeria monocytogenes: cell biology of invasion and
488 intracellular growth. Microbiol Spectr2018/12/14. 6.
489 10. Mellin JR, Koutero M, Dar D, Nahori MA, Sorek R, Cossart P. 2014. Riboswitches.
490 Sequestration of a two-component response regulator by a riboswitch-regulated noncoding
491 RNA. Science (1979) 345:940–943.
492 11. DebRoy S, Gao P, Garsin DA, Harvey BR, Kos V, Nes IF, Solheim M. 2014. Transcriptional
493 and Post Transcriptional Control of Enterococcal Gene Regulation, p. . *In* Gilmore, MS,
494 Clewell, DB, Ike, Y, Shankar, N (eds.), Enterococci: From Commensals to Leading Causes
495 of Drug Resistant Infection. Boston.
496 12. DebRoy S, Gebbie M, Ramesh A, Goodson JR, Cruz MR, van Hoof A, Winkler WC, Garsin
497 DA. 2014. Riboswitches. A riboswitch-containing sRNA controls gene expression by
498 sequestration of a response regulator. Science (1979) 345:937–940.
499 13. Chen J, Gottesman S. 2014. RNA. Riboswitch regulates RNA. Science (1979) 345:876–
500 877.
501 14. Anderson CJ, Clark DE, Adli M, Kendall MM. 2015. Ethanolamine Signaling Promotes
502 Salmonella Niche Recognition and Adaptation during Infection. PLoS Pathog
503 11:e1005278.
504 15. Anderson CJ, Satkovich J, Koseoglu VK, Agaisse H, Kendall MM. 2018. The Ethanolamine
505 Permease EutH Promotes Vacuole Adaptation of Salmonella enterica and Listeria
506 monocytogenes during Macrophage Infection. Infect Immun2018/03/14. 86.

507 16. Penrod JT, Mace CC, Roth JR. 2004. A pH-sensitive function and phenotype: evidence
508 that EutH facilitates diffusion of uncharged ethanolamine in Salmonella enterica. J Bacteriol
509 186:6885–6890.
510 17. Bobik TA, Lehman BP, Yeates TO. 2015. Bacterial microcompartments: widespread
511 prokaryotic organelles for isolation and optimization of metabolic pathways. Mol Microbiol
512 98:193–207.
513 18. Kerfeld CA, Aussignargues C, Zarzycki J, Cai F, Sutter M. 2018. Bacterial
514 microcompartments. Nat Rev Microbiol2018/03/06. 16:277–290.
515 19. Zeng Z, Boeren S, Bhandula V, Light SH, Smid EJ, Notebaart RA, Abee T. 2021. Bacterial
516 Microcompartments Coupled with Extracellular Electron Transfer Drive the Anaerobic
517 Utilization of Ethanolamine in Listeria monocytogenes. mSystems 6.
518 20. Quin MB, Perdue SA, Hsu SY, Schmidt-Dannert C. 2016. Encapsulation of multiple cargo
519 proteins within recombinant Eut nanocompartments. Appl Microbiol Biotechnol2016/07/28.
520 100:9187–9200.
521 21. Choudhary S, Quin MB, Sanders MA, Johnson ET, Schmidt-Dannert C. 2012. Engineered
522 protein nano-compartments for targeted enzyme localization. PLoS One 7:e33342.
523 22. Held M, Kolb A, Perdue S, Hsu SY, Bloch SE, Quin MB, Schmidt-Dannert C. 2016.
524 Engineering formation of multiple recombinant Eut protein nanocompartments in E. coli.
525 Sci Rep2016/04/12. 6:24359.
526 23. Kutzner E, Kern T, Felsl A, Eisenreich W, Fuchs TM. 2016. Isotopologue profiling of the
527 listerial N-metabolism. Mol Microbiol 100.
528 24. WELSHIMER HJ. 1963. VITAMIN REQUIREMENTS OF LISTERIA MONOCYTOGENES.
529 J Bacteriol 85.
530 25. Premaratne RJ, Lin WJ, Johnson EA. 1991. Development of an improved chemically
531 defined minimal medium for Listeria monocytogenes. Appl Environ Microbiol 57.

532 26. Tsai HN, Hodgson DA. 2003. Development of a Synthetic Minimal Medium for Listeria
533 monocytogenes. Appl Environ Microbiol 69.
534 27. FRIEDMAN ME, KAUTTER DA. 1962. Effect of nutrition on the respiratory virulence of
535 Listeria monocytogenes. J Bacteriol 83.
536 28. Gaillard JL, Berche P, Mounier J, Richard S, Sansonetti P. 1987. In vitro model of
537 penetration and intracellular growth of Listeria monocytogenes in the human enterocyte-
538 like cell line Caco-2. Infect Immun1987/11/01. 55:2822–2829.
539 29. Mounier J, Ryter A, Coquis-Rondon M, Sansonetti PJ. 1990. Intracellular and cell-to-cell
540 spread of Listeria monocytogenes involves interaction with F-actin in the enterocytelike cell
541 line Caco-2. Infect Immun1990/04/01. 58:1048–1058.
542 30. Rajabian T, Gavicherla B, Heisig M, Müller-Altrock S, Goebel W, Gray-Owen SD, Ireton K.
543 2009. The bacterial virulence factor InlC perturbs apical cell junctions and promotes cell-
544 to-cell spread of Listeria. Nat Cell Biol 11.
545 31. Ouadrhiri Y, Scorneaux B, Sibille Y, Tulkens PM. 1999. Mechanism of the intracellular
546 killing and modulation of antibiotic susceptibility of Listeria monocytogenes in THP-1
547 macrophages activated by gamma interferon. Antimicrob Agents Chemother 43.
548 32. Borish LC, Steinke JW. 2003. Borish, L. C., & Steinke, J. W. (2003). 2. Cytokines and
549 chemokines. The Journal of Allergy and Clinical Immunology, 111(2 Suppl), S460–S475.
550 http://doi.org/10.1067/mai.2003.1082. Cytokines and chemokines. J Allergy Clin Immunol
551 111.
552 33. Kany S, Vollrath JT, Relja B. 2019. Cytokines in inflammatory disease. Int J Mol Sci
553 https://doi.org/10.3390/ijms20236008.
554 34. Xie M, Ding C, Guo L, Chen G, Zeng H, Liu Q. 2018. Evaluation of Caco-2 cells response
555 to Listeria monocytogenes virulence factors by RT-PCR. Microb Pathog 120.

556 35. Kendall MM, Gruber CC, Parker CT, Sperandio V. 2012. Ethanolamine controls expression
557 of genes encoding components involved in interkingdom signaling and virulence in
558 enterohemorrhagic Escherichia coli O157:H7. mBio 3.
559 36. Garsin DA. 2012. Ethanolamine: a signal to commence a host-associated lifestyle?
560 mBio2012/07/05. 3:e00172–12.
561 37. Ramesh A, DebRoy S, Goodson JR, Fox KA, Faz H, Garsin DA, Winkler WC. 2012. The
562 mechanism for RNA recognition by ANTAR regulators of gene expression. PLoS
563 Genet2012/06/12. 8:e1002666.
564 38. Tsoy O, Ravcheev D, Mushegian A. 2009. Comparative genomics of ethanolamine
565 utilization. J Bacteriol.
566 39. Villa EA, Escalante-Semerena JC. 2022. Acinetobacter baumannii Catabolizes
567 Ethanolamine in the Absence of a Metabolosome and Converts Cobinamide into
568 Adenosylated Cobamides. mBio 13.
569 40. Penrod JT, Roth JR. 2006. Conserving a volatile metabolite: a role for carboxysome-like
570 organelles in Salmonella enterica. J Bacteriol 188:2865–2874.
571 41. Brinsmade SR, Paldon T, Escalante-Semerena JC. 2005. Minimal functions and
572 physiological conditions required for growth of salmonella enterica on ethanolamine in the
573 absence of the metabolosome. J Bacteriol 187:8039–8046.
574 42. Cameron JC, Wilson SC, Bernstein SL, Kerfeld CA. 2013. Biogenesis of a bacterial
575 organelle: the carboxysome assembly pathway. Cell 155:1131–1140.
576 43. Oltrogge LM, Chaijarasphong T, Chen AW, Bolin ER, Marqusee S, Savage DF. 2020.
577 Multivalent interactions between CsoS2 and Rubisco mediate α-carboxysome formation.
578 Nat Struct Mol Biol https://doi.org/10.1038/s41594-020-0387-7.
579 44. Yang M, Wenner N, Dykes GF, Li Y, Zhu X, Sun Y, Huang F, Hinton JCD, Liu LN. 2022.
580 Biogenesis of a bacterial metabolosome for propanediol utilization. Nat Commun 13.

581 45. Kennedy NW, Mills CE, Abrahamson CH, Archer AG, Shirman S, Jewett MC, Mangan NM,
582 Tullman-Ercek D. 2022. Linking the Salmonella enterica 1,2-Propanediol Utilization
583 Bacterial Microcompartment Shell to the Enzymatic Core via the Shell Protein PduB. J
584 Bacteriol 204.
585 46. Kaval KG, Singh K V, Cruz MR, DebRoy S, Winkler WC, Murray BE, Garsin DA. 2018.
586 Loss of Ethanolamine Utilization in Enterococcus faecalis Increases Gastrointestinal Tract
587 Colonization. mBio2018/05/10. 9.
588 47. Arnaud M, Chastanet A, Debarbouille M. 2004. New vector for efficient allelic replacement
589 in naturally nontransformable, low-GC-content, gram-positive bacteria. Appl Environ
590 Microbiol2004/11/06. 70:6887–6891.
591 48. Monk IR, Gahan CG, Hill C. 2008. Tools for functional postgenomic analysis of listeria
592 monocytogenes. Appl Environ Microbiol2008/04/29. 74:3921–3934.
593 49. Natoli M, Leoni BD, D'Agnano I, Zucco F, Felsani A. 2012. Good Caco-2 Cell Culture
594 Practices. Toxicology in Vitro 26.
595 50. Geissmann Q. 2013. OpenCFU, a New Free and Open-Source Software to Count Cell
596 Colonies and Other Circular Objects. PLoS One 8.
597
598

599 **FIGURE LEGENDS**

600

601 **Fig. 1: MMWB plus EA supports LMO10403s growth dependent on *eutV* and *eutB.*** (A)
602 Graphical representation of the organization and regulation of the *eut* operon in LMO. See text
603 for details. (B) Growth curve of LMO when grown in MMWB containing either glutamine (Gln) or
604 ethanolamine (EA) as a source of nitrogen. (C) Relative expression of the *eut* genes when LMO
605 bacteria were grown in the presence of EA with respect to Gln. (D) Growth curve comparison of
606 *ΔeutB and ΔeutB* complemented *(ΔeutB::eutB)* when grown in the presence of Gln or EA. (E)
607 Growth curve comparison of *ΔeutV and ΔeutV* complemented *(ΔeutV::eutV)* when grown in the
608 presence of Gln or EA. Shown is the average of three replicates and error bars represent the
609 standard deviation (SD).

610

611 **Fig 2: EUT BMCs form in medium containing EA.** TEM images showing the formation of EUT
612 BMCs when LMO was grown in MMWB with (A) Gln or EA. No such structures were visible in the
613 *ΔeutV* (B) and *ΔeutB* (C) strains grown under the same conditions. Complementation of *ΔeutV*
614 and *ΔeutB* partially restored the formation of BMC structures (B and C right panel respectively).
615 Scale bar represents 500nm and yellow asterisks indicate the BMCs.

616

617 **Fig 3: EUT BMCs can be fluorescently tagged.** Confocal images of the LMO *eutK::mCherry*
618 strain when grown in in MMWB with either EA (A) or Gln (B) as a nitrogen source. (B) Confocal
619 images of LMO strains containing the *eutK::mCherry* transgene (red) in *ΔeutV* (C) and *ΔeutB* (D)
620 backgrounds following growth in MMWB with EA. Scale bar represents 10μm.

621

622 **Fig. 4: *eut* mutants are deficient in intracellular replication:** Bacterial CFUs were quantified
623 in Caco-2 cells (A), RAW264.7 macrophages (B) and M1 polarized THP-1 macrophages (C). At

624 the indicated time points post-infection, the cells were washed, lysed, and serial dilutions of the
625 lysates were plated as described in methods. The mean of three replicates were calculated with
626 the error bars indicating the standard deviation. 2-way ANOVA with Bonferroni multiple testing
627 correction was used to calculate the significance of the indicated comparisons. *P < 0.05; **P <
628 0.01; ***P < 0.001; ****P < 0.0001.
629
630 **Fig. 5: LMO forms visible BMCs in Caco-2 cells dependent on *eutV* and *eutB*.** Caco-2 cells
631 were infected with LMO strains containing the *eutK::mCherry* transgene (red) in the wild type (A),
632 *ΔeutV* (B) and *ΔeutB* (C) backgrounds. The cells were fixed at the indicated time points and
633 stained with phalloidin to visualize actin (blue) and α-LMO antibody to visualize the bacteria
634 (green). Representative confocal images are shown. Scale bar represents 1μm.
635
636 **Fig 6: *eut* mutants increase pro-inflammatory signatures during Caco-2 infection.** Following
637 infection of Caco-2 cells with the indicated strains, host cell RNA was isolated and qRT-PCR
638 analysis revealed a significant elevation in the expression of genes encoding inflammatory
639 cytokines interleukin-1 beta (IL-1β), tumor necrosis factor-alpha (TNF-α), interleukin-6 (IL-6),
640 interleukin-8 (IL-8), and chemokines CXCL-2 and MCP-1. The mean of three replicates were
641 calculated with the error bars indicating the standard deviation. 2-way ANOVA with Bonferroni
642 multiple testing correction was used to calculate the significance of the indicated comparisons. *P
643 < 0.05; **P < 0.01; ***P < 0.001; ****P < 0.0001.
644
645 **Fig. S1: Growth curves of engineered strains in MMWB with EA or Gln.** Growth of *ΔeutV* (A)
646 and *ΔeutB* (B) mutants complemented using different *eut* promoters. (C) Growth of
647 *eutK::mCherry.*
648

649 **Fig. S2: EUT BMCs can be fluorescently tagged.** (D) LMO expressing *eutM::mCherry* showed
650 the formation of BMCs in vitro. (E) LMO expressing *eutK::mNeonGreen* also showed the
651 formation of BMCs in vitro. Scale bar represents 10μm.
652
653 **Fig. S3: LMO forms visible BMCs in Caco-2 cells dependent on *eutV* and *eutB*.** Full-frame,
654 representative, confocal images showing Caco-2 cells infected with LMO strains containing the
655 *eutK::mCherry* transgene (red) in the wild type, *ΔeutV,* and *ΔeutB* backgrounds. The cells were
656 fixed at the indicated time points and stained with phalloidin to visualize actin (blue) and an α-
657 LMO antibody to visualize the bacteria (green). Scale bar represents 10μm.
658
659 **Fig. S4: LMO does not form visible BMCs in RAW 264.7 and THP-1 cells.** Representative
660 images showing RAW 264.7 and THP-1 cells infected with the LMO strain containing the
661 *eutK::mCherry* transgene (red). The cells were fixed at the indicated time points and stained with
662 phalloidin to visualize actin (blue) and an α-LMO antibody to visualize the bacteria (green). Scale
663 bar represents 5μm.
664
665 **Table S1: Composition of minimal media (MMWB).**
666
667 **Table S2: List of bacterial strains and primers used in the study.**
668
669 **Table S3: Source data underlying figures.**
670
671 **Movie S1: Live cell imaging of EUT BMC formation**. LMO strains containing the *eutK::mCherry*
672 transgene (red) was layered onto an agarose pad made with Luria-Bertani medium containing
673 55mM EA and 200μM AdoCbl. An Olympus FV3000 confocal microscope equipped with TOKAI

674 HIT STX stage top incubator was used for acquiring a time-lapse image with an interval of 15
675 minutes per image.
676
677 **Table S1: Composition of minimal media (MMWB)**
678

Components	Concentration
$Na_2HPO4.7H_2O$	11.55mM
KH_2PO_4	4.82mM
$MgSO_4.7H_2O$	1.7mM
MOPS (pH 7.4)	100mM
Glucose	55mM
Riboflavin	1.33μM
Thiamine	2.96 μM
Biotin	2.05 μM
Lipoic acid	24pM
Methionine	0.67mM
Cysteine	0.82mM
Leucine	0.76mM
Isoleucine	0.76mM
Valine	0.85mM
Arginine	0.57mM
Histidine	0.64mM
*Glutamine	4.1mM
*Vitamin B12	200μM
*Ethanolamine	16mM

679
680 * These were added as required. Both Glutamine and Ethanolamine are used as a nitrogen
681 source. Vitamin B12 was added when Ethanolamine was used as a nitrogen source.
682
683
684 **Table S2: List of bacterial strains and primers used in the study.**
685
686 Bacterial strains
687

Strain name	Purpose	Comments
E. coli TOP10	cloning	
E. coli DH5α	cloning	
Listeria monocytogenes 10403S (LMO)	Study organism	Source: Bei Resource; wild type

LMAC030: *ΔeutV*	Study organism	*ΔeutV* constructed on LMO 10403s background
LMAC031: *ΔeutB*	Study organism	*ΔeutB* constructed on LMO 10403s background
LMAC007: *eutK::mNeonGreen*	Study organism	LMO expressing *eutK::mNG*
LMAC024: *ΔeutB::eutB(eutV promoter)*	Study organism	*ΔeutB::eutB; ΔeutB* complemented with a copy of *eutB* gene under the control of *eutV* promoter.
LMAC026: *ΔeutV::eutV(eutG promoter)*	Study organism	*ΔeutV::eutVW; ΔeutV* complemented with a copy of *eutVW* gene under the control of *eutG* promoter.
LMAC034: *ΔeutB::eutB(eutG promoter)*	Study organism	*ΔeutB::eutB; ΔeutB* complemented with a copy of *eutB* gene under the control of eutG promoter with riboswitch.
LMAC037: *ΔeutV::eutV(eutV promoter)*	Study organism	*ΔeutV::eutVW; ΔeutV* complemented with a copy of *eutVW* gene under the control of *eutV* promoter.
LMAC038: *eutK::mCherry*	Study organism	LMO expressing *eutK::mCherry*
LMAC039: *eutM::mCherry*	Study organism	LMO expressing *eutM::mCherry*
LMAC040: *eutK::mCherry*; *ΔeutV*	Study organism	LMAC030 expressing *eutK::mCherry*
LMAC043: *eutK::mCherry*; *ΔeutB*	Study organism	LMAC031 expressing *eutK::mCherry*

List of primers cloning, knockout (KO) generation, complementation (CT)

Primer sequence	Purpose	Comment
TGGGGATCGGAATTCGAGCTGACGGATGCACTGCAACAAATC	*eutV* promoter_fwd	LMAC007: *eutK::mNeonGreen*
CATTTGGCATTCTATAGAAGCATTTACTTGAGCGAAAG	*eutV* promoter_rev	
CTTCTATAGAATGCCAAATGAAGCGCTTG	*eutK* coding_fwd	
AGCTCCCGCTCCTGCGCCGTTTTCACTCCTTCCATAAATATCTTTTAG	*eutK* coding_rev	
GGCGCAGGAGCGGGAGCTATGGTGAGCAAGGGCGAGGAGGATA	mNeonGreen_fwd	

CGAATTCCTGCAGCCCGGGGTTACTTGTACAGCTCGTCCATGCCCATCAC	mNeonGreen_rev	
TGGGGATCGGAATTCGAGCTGACGGATGCACTGCAACAAATC	*eutV* promoter_fwd	LMAC024: *ΔeutB::eutB(eutV promoter)*
TTAAAATCATTCTATAGAAGCATTTACTTGAGCGAAAG	*eutV* promoter_rev	
CTTCTATAGAATGATTTTAAAAACGAATTTATTCG	*eutB* coding_fwd	
CGAATTCCTGCAGCCCGGGGTTATTTTAGGAAAATAGATGCATC	*eutB* coding_rev	
TGGGGATCGGAATTCGAGCTAGCAAATTCTTCTTGCAAG	*eutG*Promoter_fwd	LMAC026: *ΔeutV::eutV(eutG promoter)*
ACAAAATCATGAGATTACCTCCTAGTTTTTTAAAATTAAAAAAG	*eutG*Promoter_rev	
AGGTAATCTCATGATTTTGTCCTATATTGTGAC	*eutVW* coding_fwd	
CGAATTCCTGCAGCCCGGGGCTACTTCTTTGTAGCATGG	*eutVW* coding_rev	
ACAGATCTATCGATGCATGCAAAAGCAAATGATTACTCGG	*eutV* upstream_fwd	LMAC030: *ΔeutV*
ATCATGTTGTTCTATAGAAGCATTTACTTGAG	*eutV* upstream_rev	
CTTCTATAGAACAACATGATTCGTAATCTG	*eutV* downstream_fwd	
CCTCGCGTCGGGCGATATCGTCATAATAAAGTAATTCCCGG	*eutV* downstream_rev	
ACAGATCTATCGATGCATGCTTAGGTGAAATGGTTGAG	*eutB* upstream_fwd	LMAC031: *ΔeutB*
CCATTTTCGCTCGATAAATCCTCCTCTC	*eutB* upstream_rev	
GATTTATCGAGCGAAAATGGTAAATTAACTAGC	*eutB* downstream_fwd	
CCTCGCGTCGGGCGATATCGAACTGTACGACGAGCTTC	*eutB* downstream_rev	

TGGGGATCGGAATTCGAGCTAGCAAATTCTTCTTGCAAG	*eutG* promoter_fwd	LMAC034: *ΔeutB::eutB(eutG promoter)*
TTAAAATCATGAGATTACCTCCTAGTTTTTTAAAATTAAAAAAG	*eutG* promoter_rev	
AGGTAATCTCATGATTTTAAAAACGAATTTATTCG	*eutB* coding_fwd	
CGAATTCCTGCAGCCCGGGGTTATTTTAGGAAAATAGATGCATC	*eutB* coding_rev	
TGGGGATCGGAATTCGAGCTGACGGATGCACTGCAACAAATC	*eutVW-* promoter+ coding_fwd	LMAC037: *ΔeutV::eutV(eutV promoter)*
CGAATTCCTGCAGCCCGGGGCTACTTCTTTGTAGCATGGATAGAATTG	*eutVW-* promoter+ coding_rev	
TGGGGATCGGAATTCGAGCTAGCAAATTCTTCTTGCAAG	*eutG* promoter_fwd	AC038 construct. Electroporated to LMO to generate LMAC038: (*eutK::mCherry);* LMAC040 (*eutK::mCherry*; *ΔeutV*) and LMAC043(*eutK::mCherry*; *ΔeutB)*
CATTTGGCATGAGATTACCTCCTAGTTTTTTAAAATTAAAAAAG	*eutG* promoter_rev	
AGGTAATCTCATGCCAAATGAAGCGCTTG	*eutK* coding_fwd	
TACTAACCATGTTTTCACTCCTTCCATAAATATCTTTTAG	*eutK* coding_rev	
GAGTGAAAACATGGTTAGTAAAGGTGAAG	mCherry coding_fwd	
CGAATTCCTGCAGCCCGGGGTTATTTATATAATTCATCCATACCAC	mCherry coding_rev	
TGGGGATCGGAATTCGAGCTAGCAAATTCTTCTTGCAAG	*eutG* promoter-fwd	LMAC039: *eutM::mCherry*
CGTTTGCCATGAGATTACCTCCTAGTTTTTTAAAATTAAAAAAG	*eutG* promoter-rev	
AGGTAATCTCATGGCAAACGCAAACGCATTAG	*eutM* coding_fwd	
TACTAACCATTTCAGCGCTTTTTGGTAGAATTG	*eutM* coding_rev	
AAGCGCTGAAATGGTTAGTAAAGGTGAAG	*mCherry* coding_fwd	
CGAATTCCTGCAGCCCGGGGTTATTTATATAATTCATCCATACCAC	*mCherry* coding_rev	

691
692

693 List of primers used for qRT PCR:
694

Primer name	Primer sequence
ACTBqPCR1S	CACCATTGGCAATGAGCGGTTC
ACTTBqPCR1AS	AGGTCTTTGCGGATGTCCACGT
IL6qPCR1S	AGACAGCCACTCACCTCTTCAG
IL6qPCR1AS	TTCTGCCAGTGCCTCTTTGCTG
IL8qPCR1S	GAGAGTGATTGAGAGTGGACCAC
IL8qPCR1AS	CACAACCCTCTGCACCCAGTTT
IL1bqPCR1S	CCACAGACCTTCCAGGAGAATG
IL1bqPCR1AS	GTGCAGTTCAGTGATCGTACAGG
ITNFaqPCR1S	CTCTTCTGCCTGCTGCACTTTG
ITNFaqPCR1AS	ATGGGCTACAGGCTTGTCACTC
CXCL2qPCR1S	GGCAGAAAGCTTGTCTCAACCC
CXCL2qPCR1AS	CTCCTTCAGGAACAGCCACCAA
MCP1qPCR1S	AGAATCACCAGCAGCAAGTGTCC
MCP1qPCR1AS	TCCTGAACCCACTTCTGCTTGG
eutV qPCR1S	TGTTGTAGGGGAAGCGACAG
eutV qPCR1AS	GATAATTCCGCCAGCAAGCC
eutA qPCR1S	GGAGGCGTTGCAGACTGTATT
eutA qPCR1AS	CGACCACTGTTGCCCGTAT
eutB qPCR1S	GCTCATTTCGGCGTAGACCA
eutB qPCR1AS	CCGGCGCGAATTACTTGTTT
eutK qPCR1S	GCTTTCTTGGTGCCGTTGTT
eutK qPCR1AS	TTCAGTTGCCGCTTTTCCTG
eutM qPCR1S	CAAGTTGGTGGCGGTCTAGT
eutM qPCR1AS	TTGCGTCTACTTCGCTGTGT
16s qPCR1S	GGGGCTAATACCGAATGATAGAATG
16s qPCR1AS	TATGCATCGTTGCCTTGGTAG
pduA qPCR1S	TCGGGTCTGGACTGGTTACT
pduA qPCR1AS	CCACATCAGTATGCGGACGA
pduQ qPCR1S	CAGGCAAAATCCAACCGCAA
pduQ qPCR1AS	GCTGTTACTTCCGAGCCTGT

695
696
697

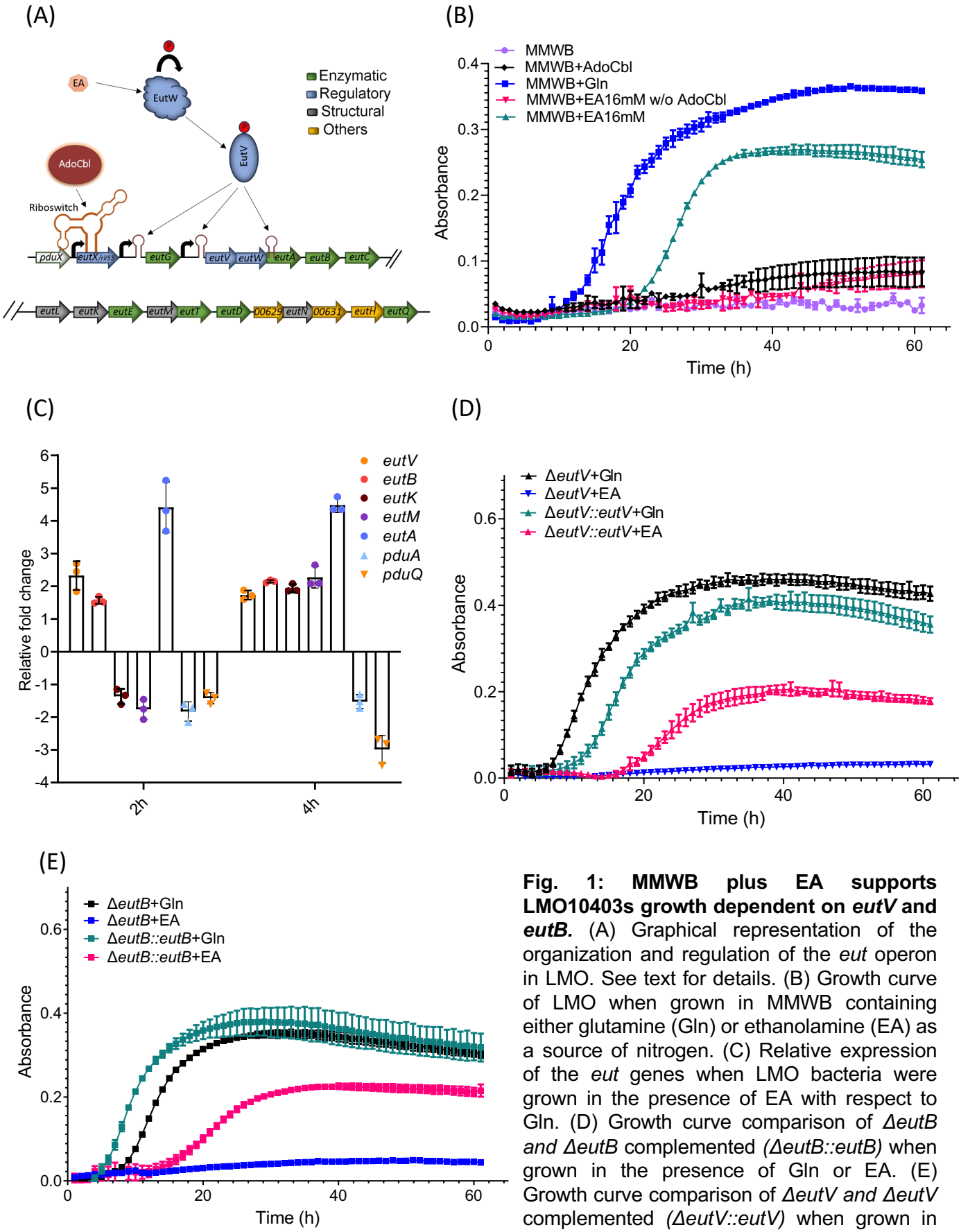

Fig. 1: MMWB plus EA supports LMO10403s growth dependent on *eutV* and *eutB*. (A) Graphical representation of the organization and regulation of the *eut* operon in LMO. See text for details. (B) Growth curve of LMO when grown in MMWB containing either glutamine (Gln) or ethanolamine (EA) as a source of nitrogen. (C) Relative expression of the *eut* genes when LMO bacteria were grown in the presence of EA with respect to Gln. (D) Growth curve comparison of *ΔeutB and ΔeutB* complemented *(ΔeutB::eutB)* when grown in the presence of Gln or EA. (E) Growth curve comparison of *ΔeutV and ΔeutV* complemented *(ΔeutV::eutV)* when grown in the presence of Gln or EA. Shown is the average of three replicates and error bars represent the standard deviation (SD).

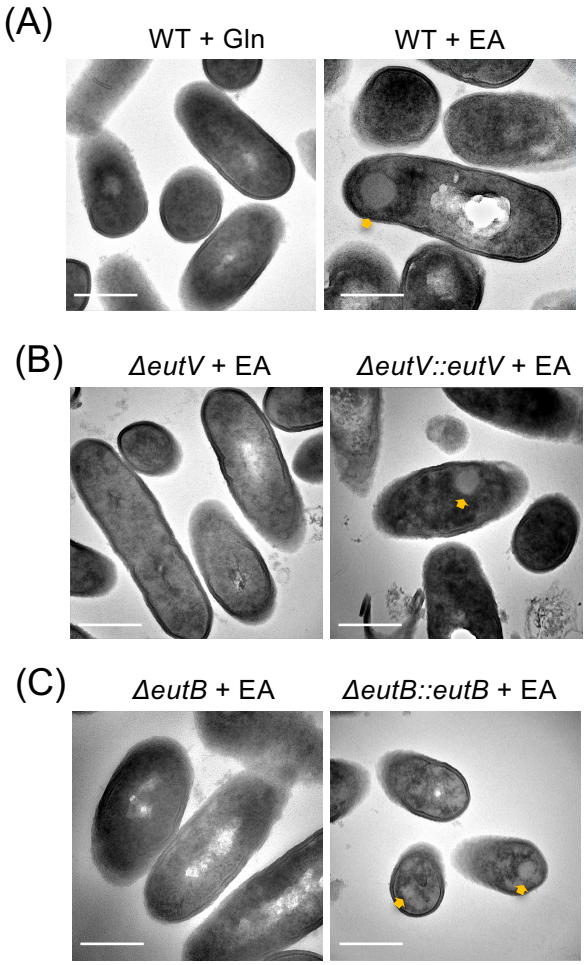

Fig 2: EUT BMCs form in medium containing EA. TEM images showing the formation of EUT BMCs when LMO was grown in MMWB with (A) Gln or EA. No such structures were visible in the *ΔeutV* (B) and *ΔeutB* (C) strains grown under the same conditions. Complementation of *ΔeutV* and *ΔeutB* partially restored the formation of BMC structures (B and C right panel respectively). Scale bar represents 500nm and yellow asterisks indicate the BMCs.

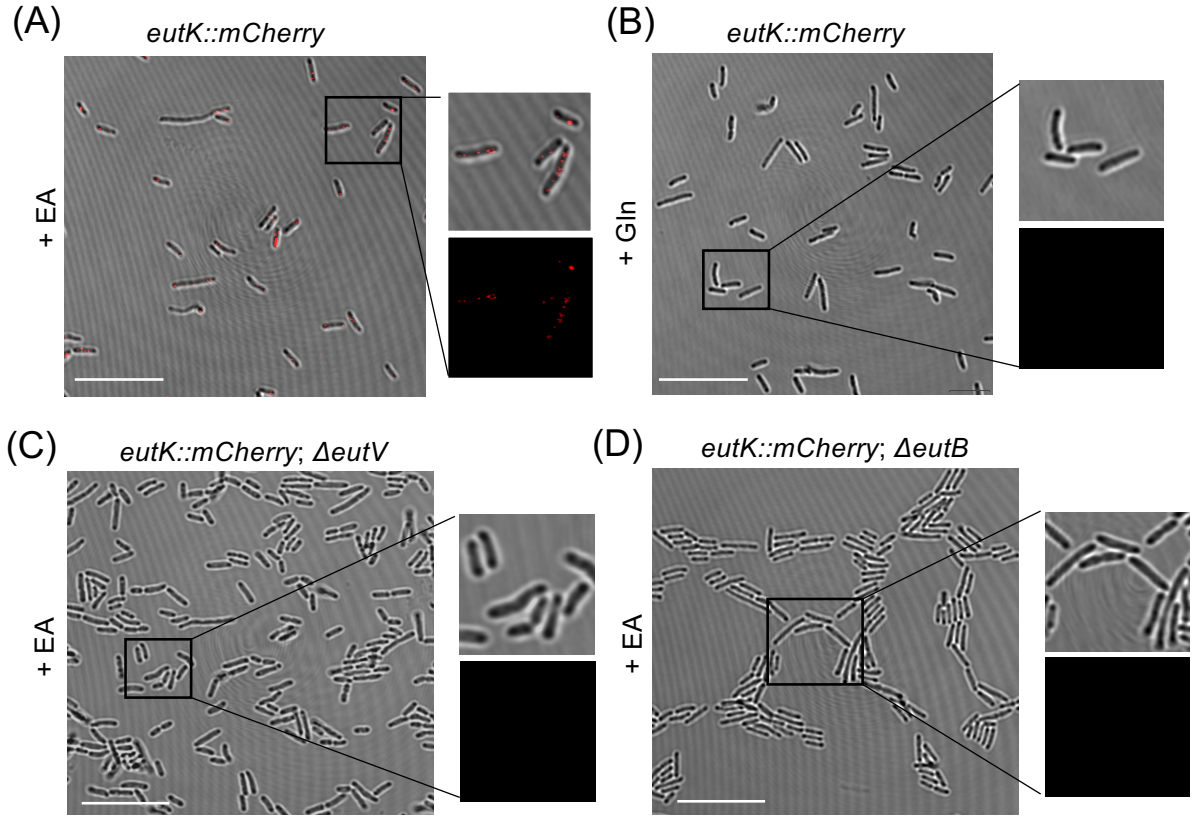

Fig 3: EUT BMCs can be fluorescently tagged. Confocal images of the LMO *eutK::mCherry* strain when grown in in MMWB with either EA (A) or Gln (B) as a nitrogen source. (B) Confocal images of LMO strains containing the *eutK::mCherry* transgene (red) in *ΔeutV* (C) and *ΔeutB* (D) backgrounds following growth in MMWB with EA. Scale bar represents 10μm.

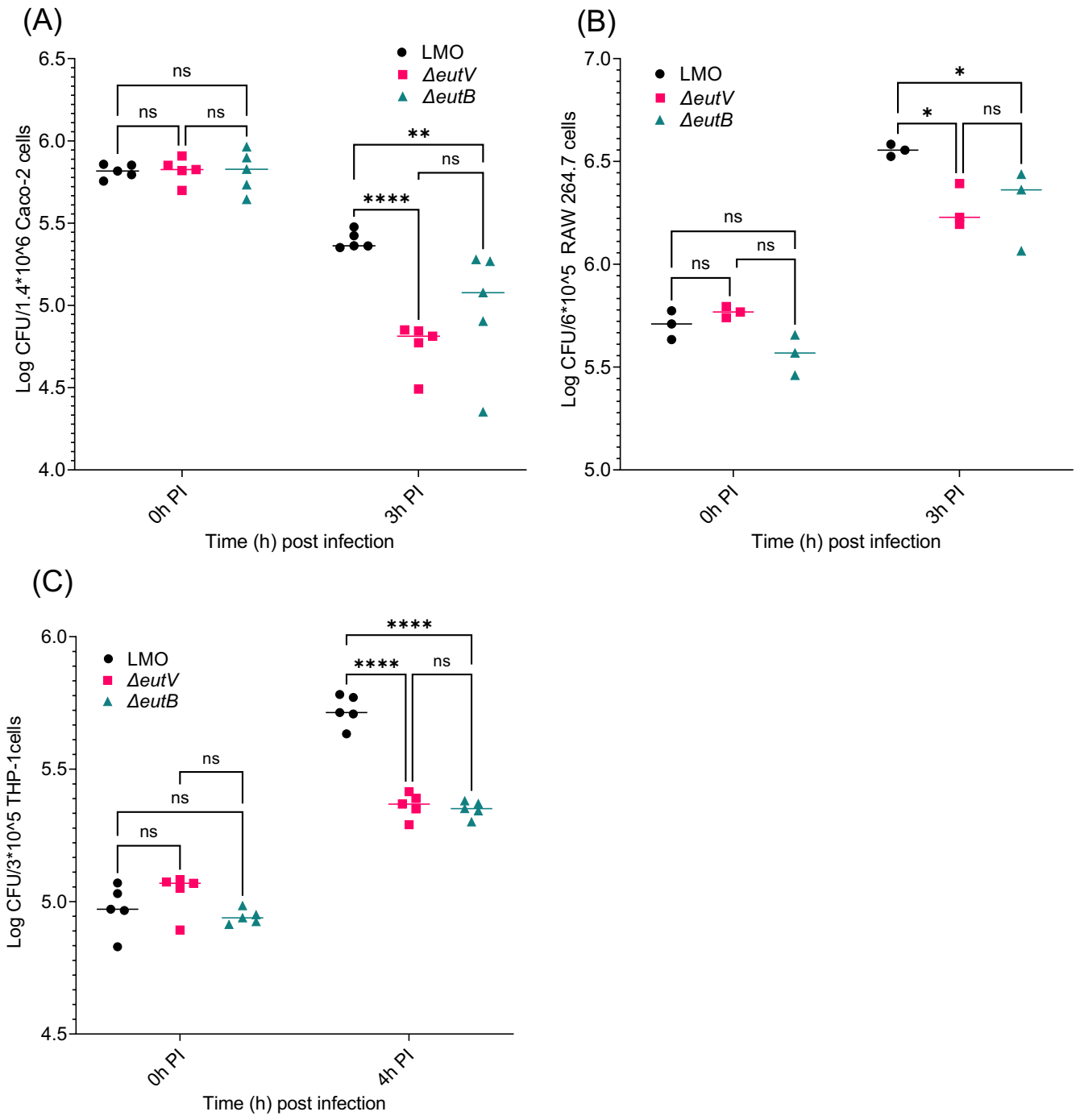

Fig. 4: *eut* mutants are deficient in intracellular replication: Bacterial CFUs were quantified in Caco-2 cells (A), RAW264.7 macrophages (B) and M1 polarized THP-1 macrophages (C). At the indicated time points post-infection, the cells were washed, lysed, and serial dilutions of the lysates were plated as described in methods. The mean of three replicates were calculated with the error bars indicating the standard deviation. 2-way ANOVA with Bonferroni multiple testing correction was used to calculate the significance of the indicated comparisons. *P < 0.05; **P < 0.01; ***P < 0.001; ****P < 0.0001.

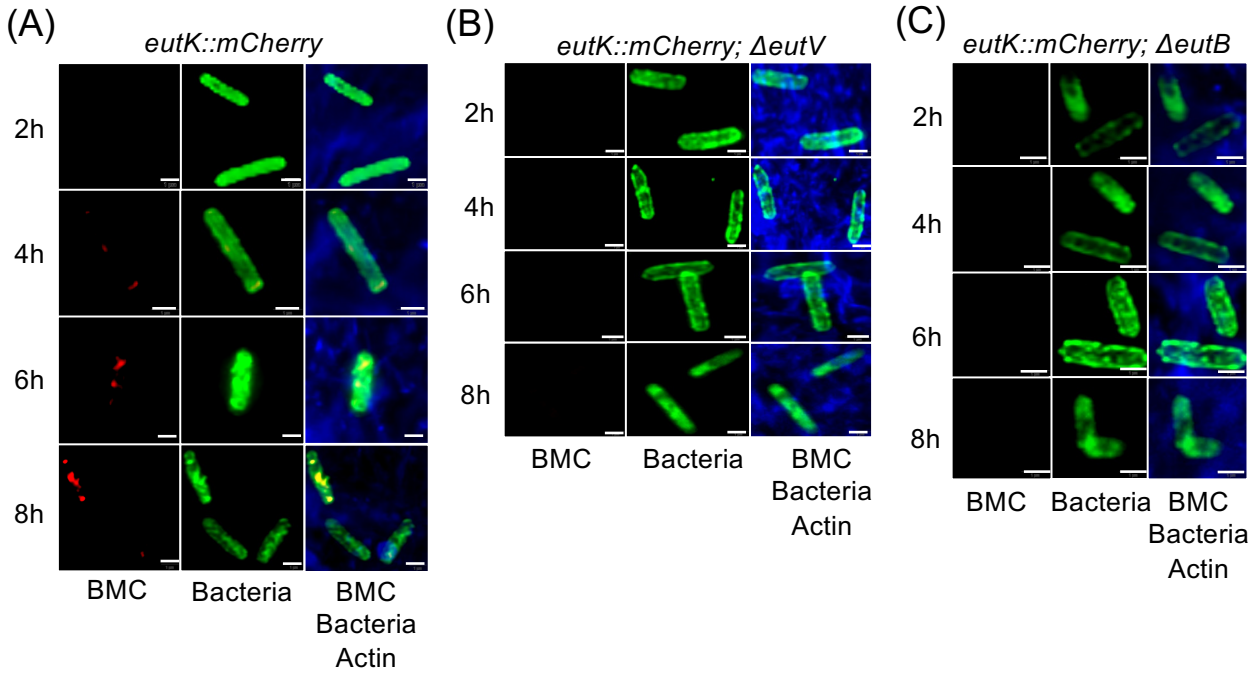

Fig. 5: LMO forms visible BMCs in Caco-2 cells dependent on *eutV* and *eutB*. Caco-2 cells were infected with LMO strains containing the *eutK::mCherry* transgene (red) in the wild type (A), *ΔeutV* (B) and *ΔeutB* (C) backgrounds. The cells were fixed at the indicated time points and stained with phalloidin to visualize actin (blue) and α-LMO antibody to visualize the bacteria (green). Representative confocal images are shown. Scale bar represents 1μm.

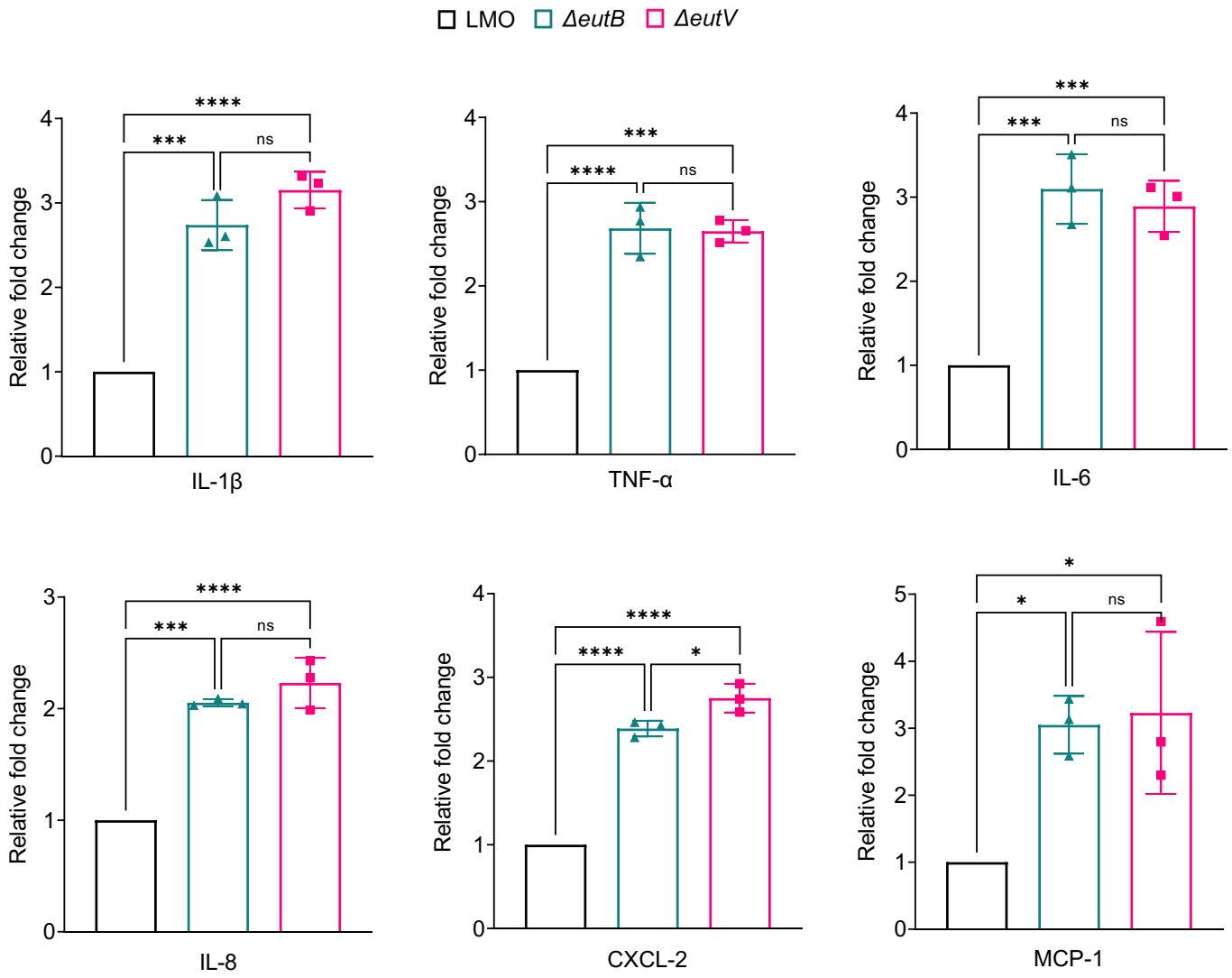

Fig 6: *eut* mutants increase pro-inflammatory signatures during Caco-2 infection. Following infection of Caco-2 cells with the indicated strains, host cell RNA was isolated and qRT-PCR analysis revealed a significant elevation in the expression of genes encoding inflammatory cytokines interleukin-1 beta (IL-1β), tumor necrosis factor-alpha (TNF-α), interleukin-6 (IL-6), interleukin-8 (IL-8), and chemokines CXCL-2 and MCP-1. The mean of three replicates were calculated with the error bars indicating the standard deviation. 2-way ANOVA with Bonferroni multiple testing correction was used to calculate the significance of the indicated comparisons. *P < 0.05; **P < 0.01; ***P < 0.001; ****P < 0.0001.

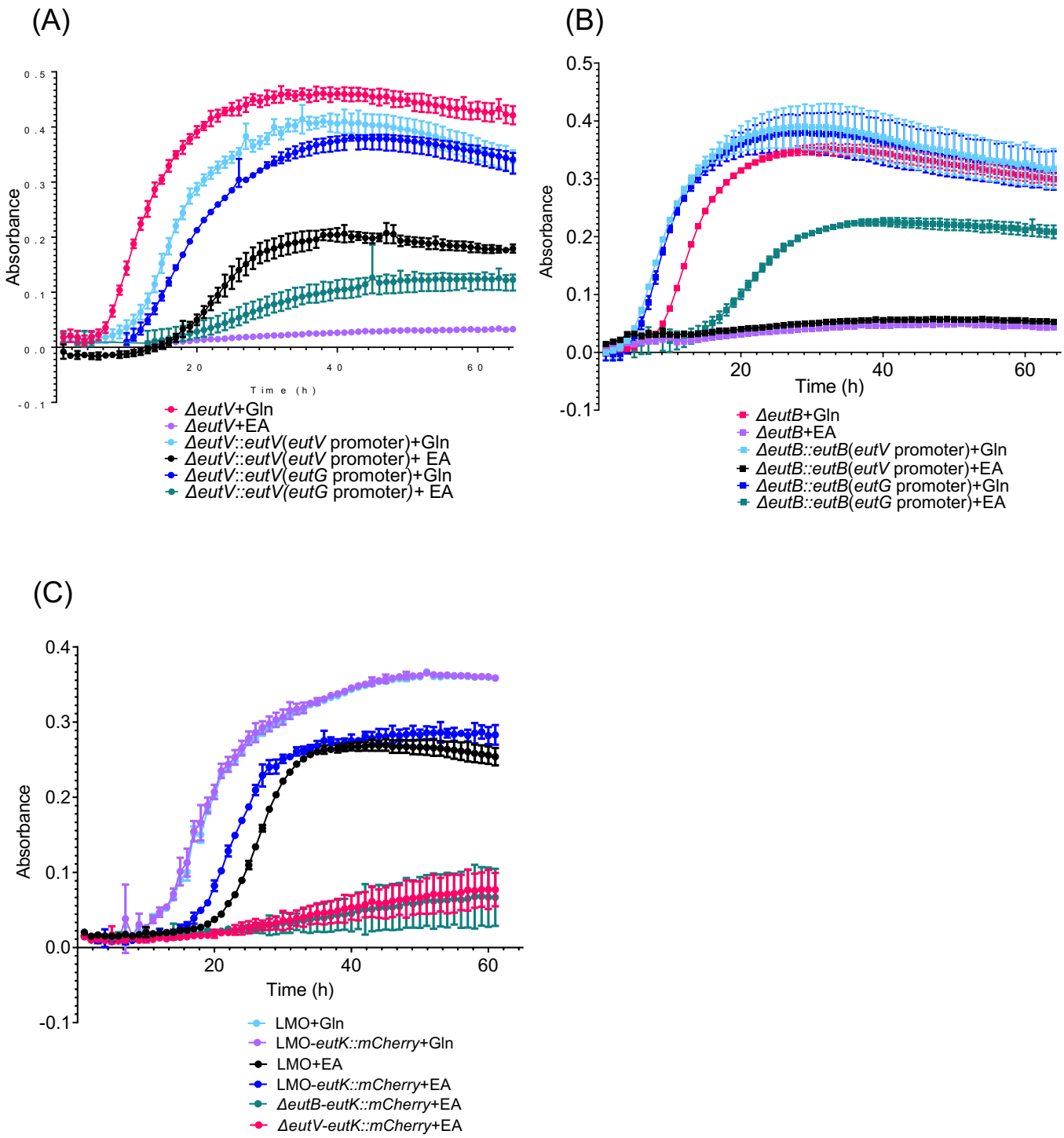

Fig. S1: Growth curves of engineered strains in MMWB with EA or Gln. Growth of *ΔeutV* (A) and *ΔeutB* (B) mutants complemented using different *eut* promoters. (C) Growth of *eutK::mCherry.*

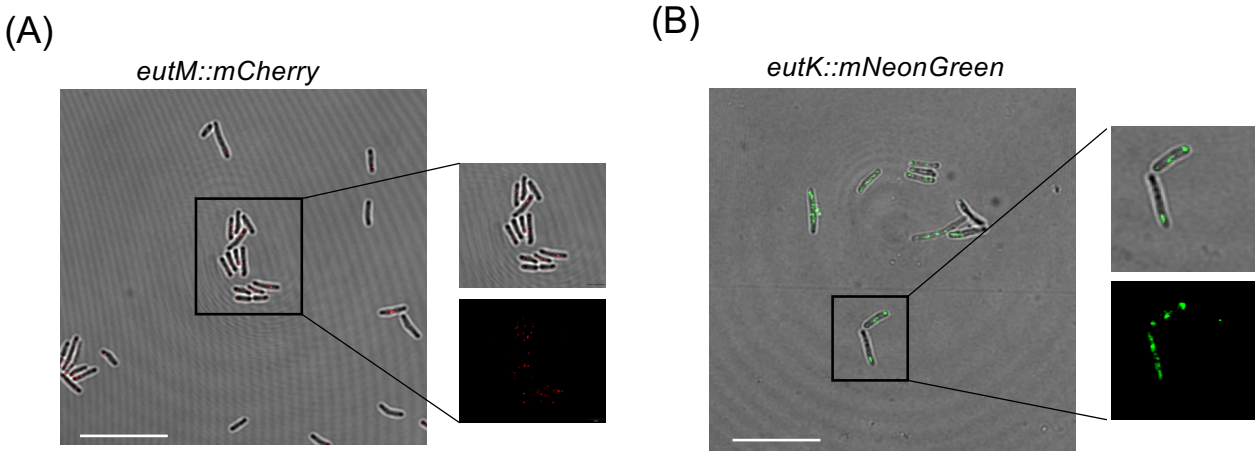

Fig. S2: EUT BMCs can be fluorescently tagged. (D) LMO expressing *eutM::mCherry* showed the formation of BMCs in vitro. (E) LMO expressing *eutK::mNeonGreen* also showed the formation of BMCs in vitro. Scale bar represents 10µm.

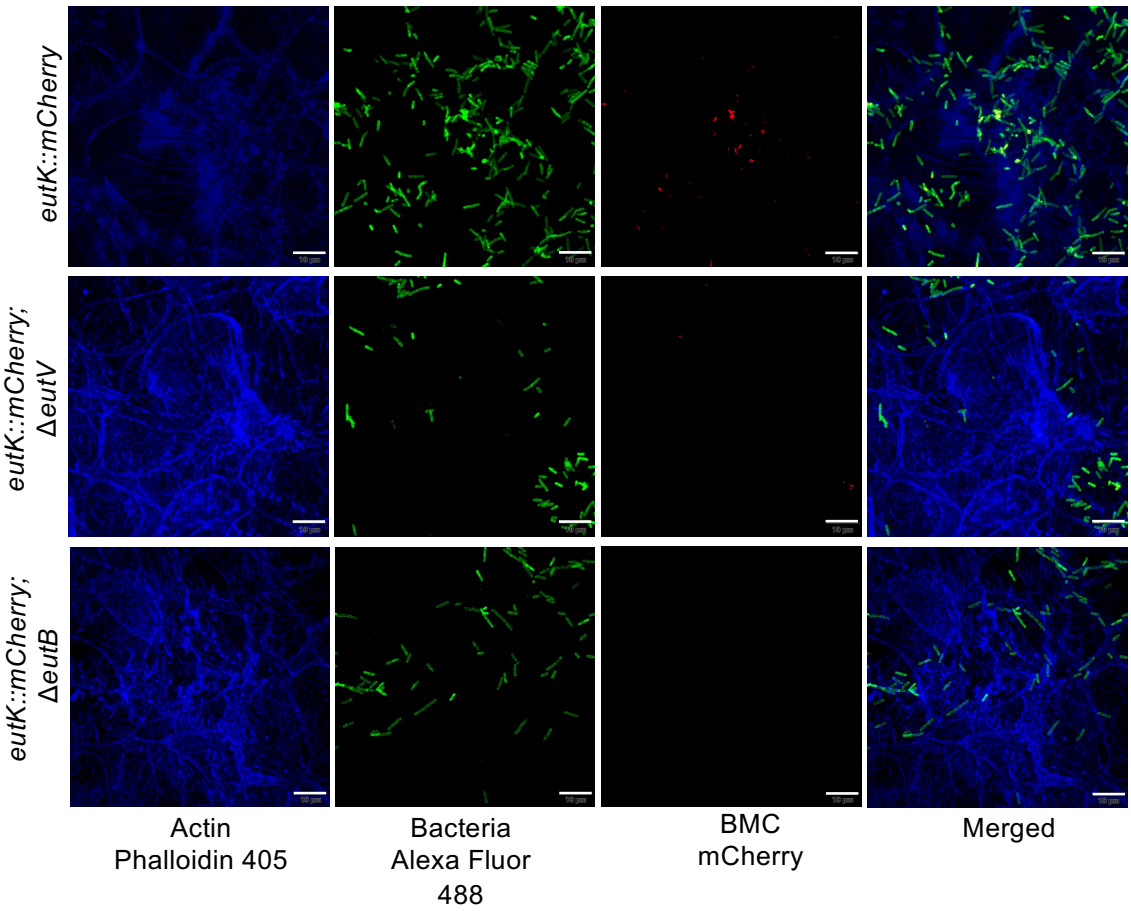

Fig. S3: LMO forms visible BMCs in Caco-2 cells dependent on *eutV* and *eutB*. Full-frame, representative, confocal images showing Caco-2 cells infected with LMO strains containing the *eutK::mCherry* transgene (red) in the wild type, *ΔeutV,* and *ΔeutB* backgrounds. The cells were fixed at the indicated time points and stained with phalloidin to visualize actin (blue) and an a-LMO antibody to visualize the bacteria (green). Scale bar represents 10μm.

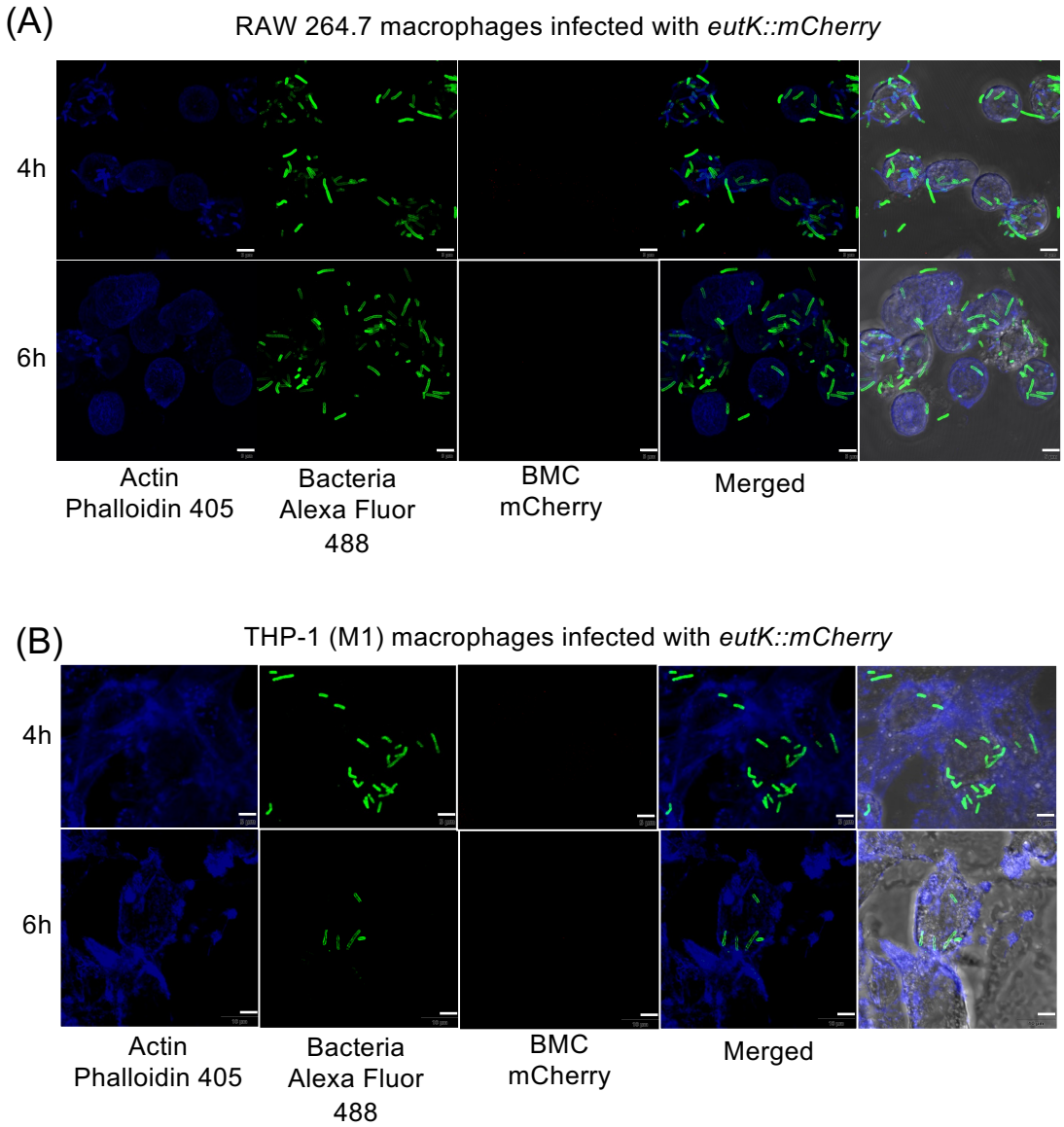

Fig. S4: LMO does not form visible BMCs in RAW 264.7 and THP-1 cells. Representative images showing RAW 264.7 and THP-1 cells infected with the LMO strain containing the *eutK::mCherry* transgene (red). The cells were fixed at the indicated time points and stained with phalloidin to visualize actin (blue) and an α-LMO antibody to visualize the bacteria (green). Scale bar represents 5μm.